Strength of $(Mg,Fe)_2SiO_4$ wadsleyite determined by relaxation of transformation stress

Jed L. Mosenfelder [a,*], James A.D. Connolly [b], David C. Rubie [a], Ming Liu [c]

[a] *Bayerisches Geoinstitut, Universität Bayreuth, D-95440 Bayreuth, Germany*
[b] *Institut für Mineralogie und Petrographie, Eidgenossische Technische Hochschule, CH-8092 Zürich, Switzerland*
[c] *Motorola Semiconductor Products Sector, MD: OE49, 6501 William Cannon Drive West, Austin, TX 78735, USA*

Abstract

The growth of a reaction rim around a crystal undergoing a polymorphic phase transformation generates elastic strain energy as a consequence of the reaction volume change. The strain energy inhibits the transformation by counteracting the chemical free energy driving force for growth. Stress relaxation enables growth to continue, at a rate controlled primarily by the mechanical properties of the rim. We studied this process in high-pressure experiments in order to constrain the rheology of wadsleyite, one of the high-pressure polymorphs of olivine. Single crystal spheres of San Carlos olivine, surrounded by a quasi-hydrostatic pressure medium of NaCl or Au, were partially transformed to wadsleyite at 1100°C and 16–17 GPa to determine the rate of growth as a function of time. Microstructural observations indicate that the relict olivine remains largely undeformed, while the wadsleyite rims deform by dislocation creep. Application of an elastoplastic model to fit the observed decrease in growth rates with time constrains the yield strength of wadsleyite at these conditions to between 4 and 6 GPa. A decrease in growth rates was also observed in another study in which varying amounts of water were added to the samples [Kubo, T., Ohtani, E., Kato, T., Shinmei, T., Fujino, K., 1998a. Experimental investigation of the α–β transformation of San Carlos olivine single crystal. Phys. Chem. Miner. 26, 1–6; Kubo, T., Ohtani, E., Shinmei, T., Fujino, K., 1998b. Effects of water on the α–β transformation kinetics in San Carlos olivine. Science 281, 85–87]. Modeling these results gives values for the yield strength of wadsleyite between 2 and 5 GPa under various conditions. A strength difference of ∼ 1 GPa is indicated by experiments at 1030°C conducted under nominally dry (200 ppm H_2O) and water-added (500 ppm H_2O) conditions, supporting the hypothesis that hydrolytic weakening is an important process in wadsleyite. The calculated yield strengths for wadsleyite indicate that it is three to six times stronger than olivine at the same conditions, based on an extrapolation of the low-temperature plasticity flow-law for olivine. These results imply a strong increase in the strength of subducting slabs in the mantle transition zone, provided that the deformation mechanism is the same as in the experiments. Furthermore, inhibition of growth by transformation stress may be an important factor in extending the depth

---

* Corresponding author. Division of Geological and Planetary Sciences, California Institute of Technology, M/C 170-25, Pasadena, CA 91125, USA.
E-mail address: jed@gps.caltech.edu (J.L. Mosenfelder).

range over which metastable olivine transforms to its high-pressure polymorphs in subducting slabs. © 2000 Elsevier Science B.V. All rights reserved.

Keywords: Wadsleyite; $(Mg,Fe)_2SiO_4$; Transformation stress

1. Introduction

The mechanical behavior of subducting lithosphere in the mantle transition zone plays an important role in controlling the dynamics of subduction and hence, the scale of mantle convection. Deformation in this part of the Earth is largely controlled by the rheology of wadsleyite and ringwoodite, the high-pressure forms of olivine (Davies, 1995; Karato, 1997). Unfortunately, the mechanical properties of these minerals are difficult to measure directly at mantle pressure–temperature conditions using existing experimental techniques (Karato and Rubie, 1997; Karato et al., 1998), although significant advances have recently been made using novel high-pressure cells (Karato and Rubie, 1997) and applying X-rays to measure stress in situ at high pressure and temperature (Chen et al., 1998). Here we describe a new method for constraining the yield strength of high-pressure phases that takes advantage of the relationship between rheology and reaction kinetics. A similar method for using stress relaxation as a rheometer was proposed by Morris (1995).

Previous theoretical studies (Honda and Sato, 1954; Christian, 1975; Morris, 1992; Liu and Yund, 1995; Liu et al., 1998) have shown that volume changes accompanying phase transformations lead to accumulation of elastic strain energy through the development of internal ''transformation stresses.'' Microstructural evidence documenting the existence of transformation strain has also been presented in many experimental studies (Carlson and Rosenfeld, 1981; Rubie and Thompson, 1985; Rubie and Champness, 1987; Gillet et al., 1987; Mosenfelder and Bohlen, 1997). Transformation strain energy inhibits reaction by raising the free energy change of the transformation. Depending on the geometry of the transforming system, this effect can substantially inhibit nucleation (Christian, 1975; Liu and Yund, 1995) and/or growth (Morris, 1992; Liu et al., 1998). Relaxation of transformation stress allows reaction to proceed, at a rate controlled by the flow properties of the phases involved (Morris, 1992).

This study addresses the effect of strain energy on growth rates, building on previous work by Liu et al. (1998) and experimental observations of Kubo et al. (1998a,b). For reactions controlled by diffusion of atoms across an interface, growth is expected to be linear with time (e.g., Turnbull, 1956). However, accumulation and subsequent relaxation of transformation stress can result in time-dependent growth rates. In a system with spherical symmetry, where the product phase of the reaction grows as a rim around the precursor phase, the stress relaxation and hence rate of growth is controlled by the rheological properties of the rim and the bulk modulus of the precursor phase, assuming elastic isotropy (Morris, 1992). Therefore, modeling changes in growth rate with time can be used to constrain the rheology of the rim phase. We have exploited this relationship in high-pressure multi-anvil experiments in which spheres of olivine were partially transformed to wadsleyite at high temperature and pressure. For comparison, we also modeled previous experimental results on the transformation of cubic olivine single crystals, conducted with differing water contents (Kubo et al., 1998a,b).

2. Experimental and analytical methods

Experiments were performed in a 1200-ton multi-anvil press at 16–17 GPa, 1100°C (Table 1) using pressure assemblies consisting of a Cr-doped MgO octahedron containing a $LaCrO_3$ resistance heater. We used 14-mm edge length octahedra and 8-mm truncated edge length (TEL) WC cubes for experiments at 16 GPa. For experiments at higher pressures, 10-mm octahedra and 5-mm TEL cubes were employed. The 14-mm assembly contains a stepped furnace designed to reduce the temperature gradient. Temperature was measured with W3%Re–W25%Re thermocouples, inserted axially, with no correction made for the effect of pressure on EMF. We calibrated pressure at 1200°C in both assemblies using the $\alpha–\beta$ Mg_2SiO_4 (Morishima et al., 1994),

Table 1
Experimental conditions and results

Run number	Reaction time (min)	Rim width (μm)
17 GPa, 1100°C		
#1852	15	27 ± 6[a]
#1820	30	57 ± 19[a]
#1978	30	48 ± 16
#1826	60	91 ± 9[a]
#1819	120	101 ± 25[a]
16 GPa, 1100°C		
#2178	15	17 ± 5
#2041	30	21 ± 6
#2045	60	67 ± 8
#2049	90	114 ± 13
#2167	120	76 ± 22
#2062	180	103 ± 13

[a] Previously reported rim widths for these samples (Liu et al., 1998) have been re-evaluated (see text).

$\beta-\gamma$ Mg_2SiO_4 (Katsura and Ito, 1989) and coesite–stishovite (Zhang et al., 1996) transitions. Note that some of the experiments conducted using the 10-mm assembly were previously reported with an estimated pressure of 16 GPa (Liu et al., 1998). Since then, new calibrations have been conducted and the pressure was re-estimated to be 17 GPa. Pressure and temperature uncertainties are considered to be ± 0.5 GPa and $\pm 30°C$, respectively.

The starting material for each experiment was a single crystal of $Mg_{1.8}Fe_{0.2}SiO_4$ San Carlos olivine, fabricated in the form of a 500-μm diameter sphere using an air abrasion method (Agee and Walker, 1988). All samples were cut from the same single crystal. We used a Bruker Fourier-transform infrared (FTIR) spectrometer to examine the hydrogen content of the crystal; details of the instrument specifications and operating procedures are presented in Kohlstedt et al. (1996). Polarized spectra on an oriented, 600-μm thick section revealed no evidence for hydrogen down to the detection limit of our spectrometer (estimated to be ~ 10 H/10^6 Si for this sample thickness and set of operating conditions).

In the experiments at 17 GPa, the spheres were embedded in a matrix of NaCl and contained in a Mo capsule 1.6 mm in diameter by 1.2 mm in length (Fig. 1A). The capsules were vacuum-dried at 225°C for at least 1 h prior to mechanical sealing. NaCl was chosen as a pressure medium because of its low strength at high temperatures and pressures (Rubie et al., 1993; Weidner et al., 1994; Ando et al., 1997), resulting in a quasi-hydrostatic pressure environment. A similar technique was employed in the experiments of Kubo et al. (1998a,b) (Fig. 1C). Tests using the NaCl pressure medium show that it has no detectable effect on the pressure calibration under the conditions of the experiments. Note that this experimental configuration has another advantage over the experiments described by Liu et al. (1998), in which single crystals embedded in a matrix of hot-pressed olivine (Fig. 1D) were transformed to wadsleyite and ringwoodite. In those experiments, the volume change associated with transformation of the hot-pressed olivine matrix to ringwoodite may have resulted in a pressure drop that was not compensated for by the hydraulic system, resulting in a higher pressure uncertainty (see Rubie, 1999 for further discussion).

For the experiments at 16 GPa, the olivine spheres were inserted into Au capsules, 1 mm in diameter by 1 mm in length, which were then placed into 1.6 mm by 1.6 mm Mo capsules filled with powdered Pyrex glass (Fig. 1B). Au is believed to be nearly as
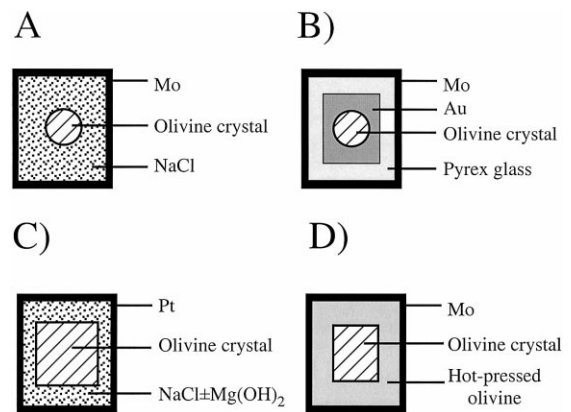

Fig. 1. Schematic view of different capsule assemblies using in kinetic experiments. (A) Mo capsule with NaCl pressure medium used in experiments at 17 GPa. (B) Mo–Pyrex–Au assembly used in experiments at 16 GPa. (C) Assembly used by Kubo et al. (1998a,b). Single crystal of olivine is embedded in NaCl or NaCl with variable proportions of $Mg(OH)_2$, used to provide a fluid source. (D) Capsule assembly used in the study of Kerschofer et al. (1996) consisting of an oriented single crystal of olivine in a matrix of hot-pressed olivine.

effective in maintaining a quasi-hydrostatic pressure environment as NaCl (cf. Weidner et al., 1992). Pyrex glass was used as an attempted ''getter'' for hydrogen that might infiltrate the sample from outside the capsule and influence the kinetics. The possible influence of trace amounts of fluids on the transformation is discussed in Section 5.2.

Following transformation, all experiments were quenched to less than 400°C in 1–2 s by cutting power to the furnace. The recovered samples were separated from the capsule material and mounted in crystal bond in order to make 30-μm thin sections, cut precisely through the middle of the spheres. Optical microscopy was used to examine reaction textures and measure growth distances. Selected samples were also ion-thinned for examination using a Philips CM20-FEG transmission electron micro-

scope (TEM) operating at 200 kV. The reported growth distances (see Table 1) represent the average and standard deviation of 10–20 measurements for each sample; note that the values differ slightly for some experiments previously reported in Liu et al. (1998) due to the more rigorous measuring procedure adopted here.

3. Experimental results

3.1. Reaction and deformation textures

Thin sections of the recovered samples show that the reaction product nucleates on the surface of the sphere and grows progressively inward with time, forming a ''reaction rim'' (Fig. 2), consisting pre-
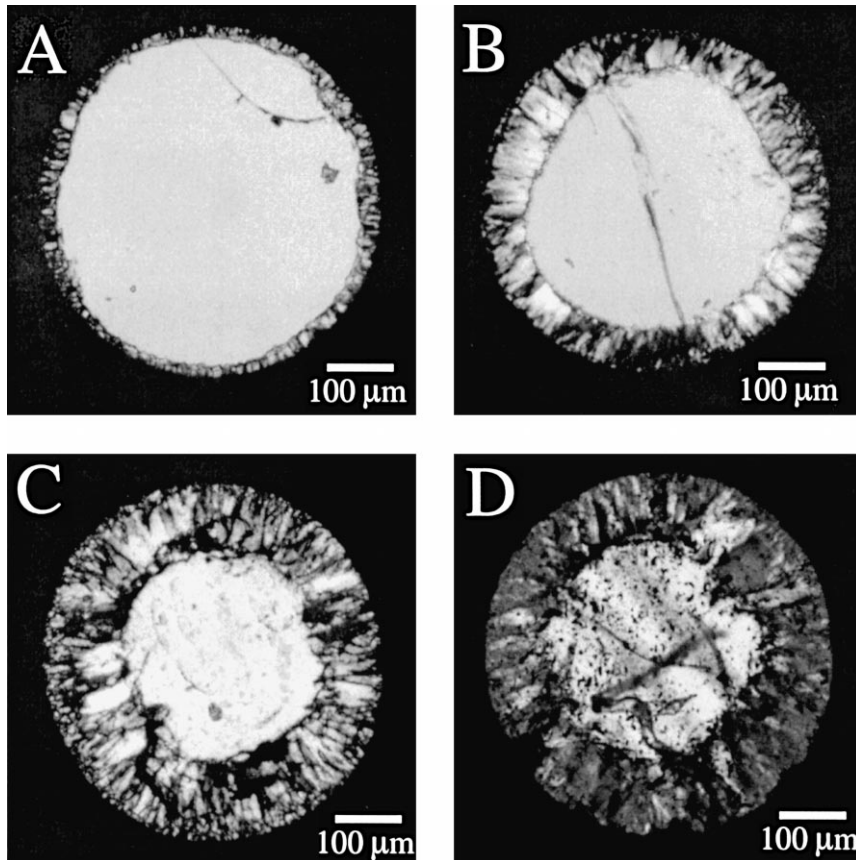

Fig. 2. Optical photomicrographs (crossed–polarized light) showing reaction rims of wadsleyite growing into spherical olivine crystals. All samples transformed at 16 GPa, 1100°C, using Au pressure medium for times of (A) after 30 min, (B) 60 min, (C) 90 min, (D) 180 min.

dominantly of wadsleyite. In contrast to samples transformed at pressures ≥ 18 GPa (Kerschhofer et al., 1996; Martinez et al., 1997; Mosenfelder et al., unpublished results), nucleation did not occur in the interior of the olivine single crystals in this study. Lack of intracrystalline transformation at the lower pressure conditions of this study may reflect the difficulty in overcoming the high strain energy inhibiting nucleation. This result is consistent with the calculations of Liu and Yund (1995), which indicate that the activation energy for nucleation decreases substantially at high-pressure oversteps because the strain energy inhibiting nucleation is overcome by chemical free energy.

Although there is no lattice-preferred orientation in the wadsleyite or epitaxial relationship between the wadsleyite and olivine, the crystals comprising the rim typically exhibit a shape-preferred orientation, with elongation perpendicular to the surface of the sphere. Electron microprobe analyses reveal no changes in Fe–Mg ratio between the phases. Similar textures have been observed in many other studies (e.g., Remsberg et al., 1988; Young et al., 1993; Kerschhofer et al., 1996; Kubo et al., 1998a,b) and interpreted as evidence for an interface-controlled nucleation and growth mechanism. The shape-preferred orientation may reflect a simple geometrical constraint imposed on the growth direction as a result of impingement of wadsleyite grains by other grains growing inward from the rim. Alternatively, it may be related to the orientation of the stress field in the rim (cf. Green et al., 1992), because the radial component of the deviatoric stress is effectively tensile while the tangential component is compressive (see below for further discussion).

Because the conditions of the experiments are nominally in the two-phase wadsleyite + ringwoodite stability field (Katsura and Ito, 1989), both phases are expected to be present. However, ringwoodite was not found in samples transformed at 16 GPa. This may be due either to a nucleation barrier for ringwoodite or to a discrepancy between the pressure calibration and the phase diagram of Katsura and Ito (1989). In some samples transformed at 17 GPa, small crystals of ringwoodite 50–200 nm in size have been detected using TEM. These crystals nucleate and grow inside much larger wadsleyite crystals and have the same epitaxial relationship with wads-

leyite determined by Dupas-Bruzek et al. (1998a). The growth of ringwoodite thus appears to be a secondary event occurring after the initial growth of the wadsleyite rim at the expense of olivine.

We used TEM to investigate deformation microstructures in our samples (Fig. 3). Dislocation densities in olivine are low, suggesting that pressure remained nearly hydrostatic in the interior of the samples. Wadsleyite grains comprising the rim contain a high density of (010) stacking faults broken up by closely spaced dislocation cell walls, but few free dislocations. Stacking faults are common in wadsleyite and may represent either growth defects or deformation-induced defects, depending on the displacement along the (010) plane (Price, 1983; Sharp et al., 1994; Dupas-Bruzek et al., 1998a). The presence of organized cell walls suggests that dislocation climb is rapid, even at the relatively low temperature of the experiments. This finding is consistent with the study of Dupas-Bruzek et al. (1998a), who observed evidence for dislocation climb in wadsleyite at 900°C. These features indicate that deformation occurred by dislocation creep, although it is not clear whether the rate of climb or the rate of glide was rate-controlling (see discussion below). No evidence
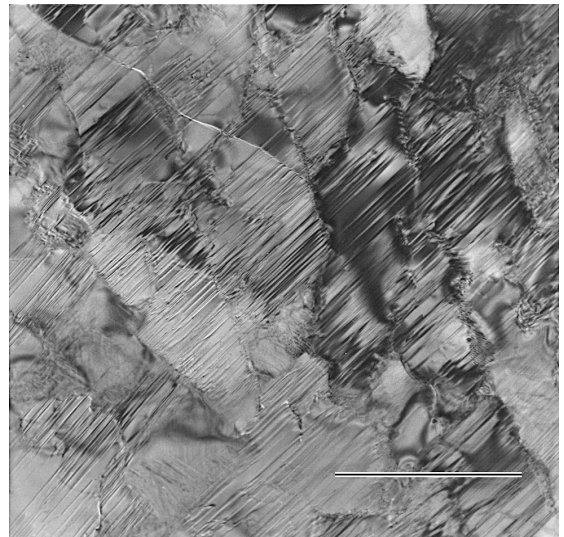

Fig. 3. Bright-field TEM photograph showing typical microstructures of wadsleyite rim in sample reacted at 1100°C, 17 GPa, for 60 min (sample 1826). The wadsleyite grains contain numerous (010) stacking faults intersected by closely spaced subgrain boundaries. Scale bar = 1 μm.

was found in any samples for deformation by diffusion creep or grain boundary sliding (e.g., four-grain junctions or equi-axed, fine-grained crystals with low dislocation densities; Ashby and Verrall, 1973).

3.2. Growth rates

Rim width measurements show that the growth rate decreases with time (Table 1, see also Fig. 5). According to the theory of Turnbull (1956), the rate of growth in polymorphic transformations is controlled by the diffusion of atoms across the interface between reactant and product and should be linear with time. Interface-controlled growth has been modeled using the following equation (Turnbull, 1956; Rubie and Ross, 1994):

$$\dot{x} = k_0 T \exp\{-[\Delta H_a + PV^*]/RT\}$$
$$\times \{1 - \exp[\Delta G_{rxn}/RT]\} \qquad (1)$$

where k_0 is a constant, T is absolute temperature, ΔH_a is the activation enthalpy for growth, P is pressure, V^* is an activation volume, R is the gas constant, and ΔG_{rxn} is the free energy of reaction. In this study, V^* was estimated using the model of Rubie and Ross (1994), and ΔG_{rxn} was calculated using the thermodynamic data of Akaogi et al. (1989). Note that ΔG_{rxn} can be modified for purposes of the model presented below by incorporating a term for strain energy. Activation energy parameters for Eq. 1 were determined by Liu et al. (1998) based on their analysis of growth rates in fine-grained $(Mg_{1.8}Fe_{0.2})SiO_4$ aggregates, where strain energy is unlikely to be an important effect. The parameters determined by Liu et al. (1998) are close to those determined by analysis (Mosenfelder et al., in preparation) of transformation experiments on Fo100 by in situ X-ray diffraction experiments (Kubo, 1998). We have used slightly different parameters because the measured growth rates in our experiments for small amounts of transformation (after 15 min) were faster than those predicted using their values (e.g., 3.55×10^{-8} vs. 3.0×10^{-8} m s^{-1} at 17 GPa and 1100°C). These differences in growth rates may be due to differing trace amounts of water in the samples, and/or differences in the pressure of the experiments.

4. Model for time-dependent growth rates

In this section, we present the outline of a model for the effect of transformation strain energy on growth kinetics that can be used to constrain the rheology of the high-pressure reaction rims. The full mathematical derivation of the model is given in Appendix A. The modeling strategy involves determining the strain energy of the system as the rim grows — for a given model rheology — and adding this quantity to the ΔG_{rxn} term in Eq. 1 to predict the growth as a function of time.

The instantaneous elastic response to the misfit strain that arises as a consequence of the volume change associated with the olivine–wadsleyite reaction produces differential stresses that may relax by viscoplastic deformation. Provided that both phases are rheologically isotropic, stresses in the olivine ''inclusion'' remain hydrostatic during growth of the wadsleyite rim. Deviatoric stresses develop in the rim, however, and the differential stress decays asymptotically away from the interface between the two phases (Fig. 4; Hill, 1950). It follows that viscoplastic relaxation is confined to the rim. To avoid the complexity associated with a viscoelastic model (e.g., Morris, 1995), we adopt a model for relaxation by ideal plastic yielding. Justification for this simplification lies in the exponential dependence of strain rate on differential stress for deformation by low-temperature plasticity (e.g., Frost and Ashby, 1982). Because of this dependence, the range of differential stresses at which the mechanism operates for a given strain rate is narrow and therefore reasonably approximated by a fixed yield strength.

The formulation of our elasto-plastic model follows the work of Lee et al. (1980), who solved for the stress field of a misfitting inclusion growing in an elastoplastic matrix (the reverse problem from that considered here, where the product grows inward from the rim). In the model, a spherical inclusion of radius $a(1 + \varepsilon)$ is introduced into a spherical hole in a matrix of radius R, giving rise to a misfit strain ε, given by (Liu et al., 1998):

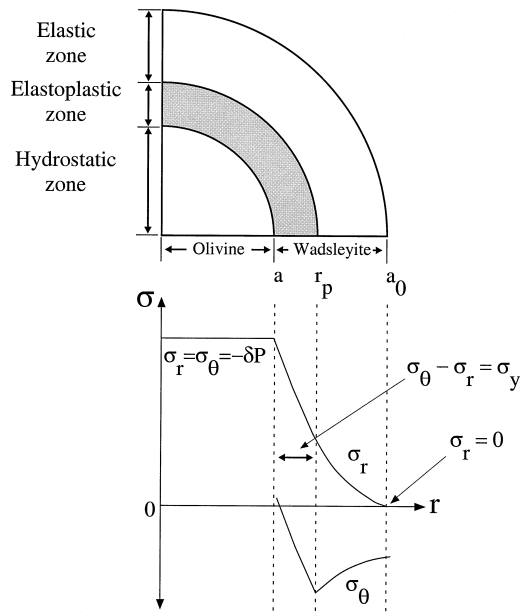$$\varepsilon = \frac{a_0^3 - a^3}{3a^3} \frac{\Delta V}{V_{rim}} \qquad (2)$$

Fig. 4. Schematic representation of the elastoplastic model. Upper portion of figure represents one quarter of the sphere; lower portion is a graph showing the development of radial and tangential stresses as a function of radius in the system. A zone of elastoplastic deformation develops in the rim when the differential stress ($\sigma_\theta - \sigma_r$) exceeds the yield strength (σ_y) of the wadsleyite. The stresses in the relic olivine are hydrostatic.

where ΔV is the molar volume change of the transformation, V_{rim} is the molar volume of the rim phase (wadsleyite), and a_0 is the initial radius of the olivine sphere. In contrast to the model of Lee et al. (1980), which assumes an infinite matrix, the rim has a finite thickness. Consequently, the boundary condition stipulated by Lee et al. (1980), that the deviatoric components of the stress tensor vanish at infinite distance from the inclusion, is inapplicable and must be replaced by a constant pressure boundary condition at the interface with the pressure medium at $r = R$. With this modification, three cases are possible in the model:

(i) At a small misfit strain, the differential stress in the rim is below the yield strength and deformation is purely elastic.
(ii) At a moderate misfit strain, the differential stress at $r = R$ is below the yield strength, but rises to the yield strength at $r_p < R$. This gives rise to a zone of elastoplastic deformation at $a < r$

$< r_p$. Within this zone the differential stress is constrained by the yield condition to be identical to the yield strength (Fig. 4).
(iii) At a large misfit strain, the elastoplastic zone encompasses the entire shell.

The solutions for these three cases are derived in Appendix A. The accumulation of strain energy as a function of time can be computed by calculating the stress and strain state of the system. The total strain energy of the system (W_{tot}) can be incorporated into the ΔG_{rxn} term in Eq. 1 as follows (cf. Liu et al., 1998):

$$\Delta G_{rxn} = \frac{4}{3}\left(a_0^3 - a^3\right)\Delta G_V^{wd-ol}(P) + W_{tot} \qquad (3)$$

where $\Delta G_V^{wd-ol}(P)$ is the chemical free energy change for a unit volume of olivine transformed to wadsleyite at the hydrostatic pressure P.

Our computational procedure consists of four iterative steps: (i) the growth rate of the wadsleyite shell is computed from Eq. 1, using the free energy term from Eq. 3; (ii) the strain energy of the olivine–wadsleyite system is computed from the elastoplastic model; (iii) the radius of the olivine is incremented by, $\dot{x}\delta t$, where δt is the magnitude of the time step, and the misfit strain (Eq. 2) recomputed; (iv) the model time is incremented.

5. Discussion

5.1. Estimate of wadsleyite strength and comparison with olivine

Model results assuming various yield strengths are shown in Figs. 5–7. The calculations were performed using values of $a_0 = 250$ μm (Eq. 2) for our experiments on 500-μm diameter spheres, and $a_0 = 500$ μm for the experiments conducted by Kubo et al. (1998a,b) on 1-mm³ cubic crystals. Note that the approximation of spherical geometry in the latter case may result in some uncertainty due to increased stresses at the corners of the samples, although we expect this effect to be small (cf. Liu et al., 1998). Furthermore, reference to Fig. 3 in Kubo et al. (1998a) suggests that not all of their samples were
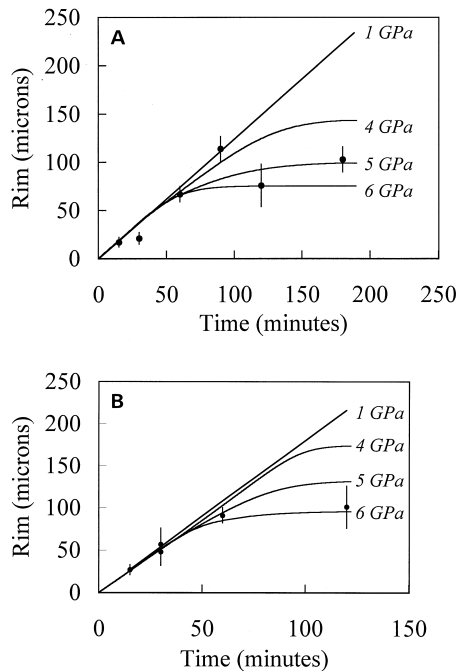
Fig. 5. (A) Model fits to results of experiments performed on spheres at 16 GPa, 1100°C, using Au/Pyrex pressure media. (B) Fits to results experiments performed at 17 GPa, 1100°C, using NaCl pressure media.
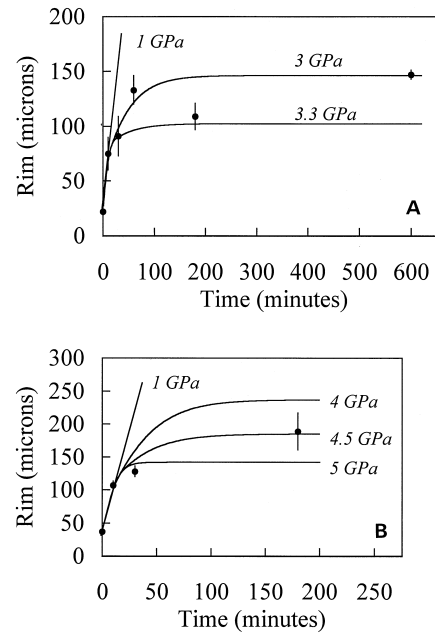

Fig. 6. Model fits to results of experiments of Kubo et al. (1998a,b) conducted under nominally dry conditions at (A) 1230°C, 14 GPa and (B) 1330°C, 15 GPa.

precisely cut into 1-mm^3 cubes; the radii assumed in our calculations may therefore be slightly overestimated.

Yield strengths of 4 to 6 GPa provide the best fits to our data on spherical olivine samples transformed to wadsleyite at 16 and 17 GPa (Fig. 5). We also fit the data of Kubo et al. (1998a,b), deriving values for the yield strength between 3 and 5 GPa for nominally dry experiments at 1030°C to 1330°C (Figs. 6, 7) and 2 to 2.5 GPa for experiments at 1030°C with water added (Fig. 7). Note that the data of Kubo et al. (1998a,b) are difficult to model using the activation energy parameters from Liu et al. (1998), presumably because the intentional addition of water in their experiments (see below) had a catalytic effect on growth kinetics. Moreover, Kubo et al. (1998a,b) observed small amounts of growth in ''zero-time'' experiments, as a result of transformation occurring during ramping to the final temperature conditions. In modeling their data, we therefore used appropriate parameters for Eq. 1 based simply on the amount of

growth that occurred in the shortest duration experiments (after time 0) at a given temperature. Finally, we note that comparison of the results of Kubo et al. (1998a,b) to ours is complicated by the use in their studies of Pt–Rh thermocouples, which may suffer a significantly different effect of pressure on EMF
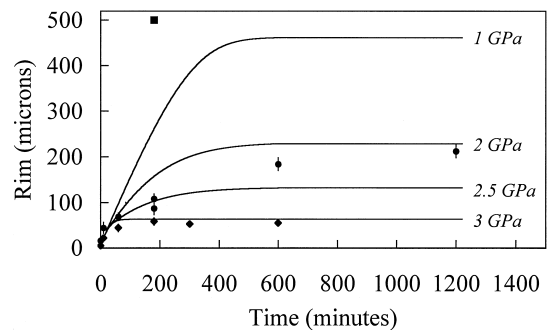

Fig. 7. Model fits to results of experiments of Kubo et al. (1998a,b) at 1030°C, 13.5 GPa, conducted under nominally dry and fluid-added conditions. Diamonds = nominally dry; circles = pressure medium consisting of 500:1 ratio of NaCl to Mg(OH)$_2$; square = pressure medium consisting of 10:1 ratio of NaCl to Mg(OH)$_2$. Some uncertainties are smaller than the data symbols.

than the W–Re thermocouples used in our experiments (see Rubie, 1999, for review).

Taken together, these results can be compared to the strength of olivine by extrapolating existing flow-laws for olivine to the conditions of the experiments. The dominant deformation mechanism for olivine at the low-temperature, high-stress conditions of the experiments is low-temperature plasticity. This mechanism has been modeled using the following flow-law (Frost and Ashby, 1982):

$$\dot{\varepsilon} = \dot{\varepsilon}(\sigma/\mu)^2 \exp\left\{-\left[(F_0 + PV^*)/RT\right]\right.$$
$$\left. \times \left[1 - (\sigma/\sigma_p)^{3/4}\right]^{4/3}\right\} \qquad (4)$$

For our extrapolation, we used the same parameters as Liu and Yund (1995): a pre-exponential constant $\dot{\varepsilon}_0$ of 8.6×10^{14} s^{-1}, activation energy F_0 of 535 kJ mol^{-1}, activation volume V^* of 2 cm^3 mol^{-1}, and Peierl's stress $\sigma_p = \sigma_0 + \psi P$, where $\sigma_0 = 8.2$ GPa and the parameter $\psi = 0.17$. For a strain rate of 10^{-6} s^{-1}, equivalent to the maximum strain rate calculated by our elastoplastic model during rim growth (at 16 GPa confining pressure with a yield strength of 4 GPa), this results in a yield strength for olivine of ~ 1 GPa. Thus, our results suggest that wadsleyite is three to six times stronger than olivine at comparable conditions. The increase in strength is consistent with deformation experiments in the power-law creep regime on analogue phases in the Mg_2GeO_4 system (Vaughan and Coe, 1981; Dupas-Bruzek et al., 1998b), which found that the spinel phase is about three times stronger than the olivine phase.

Our results are also roughly comparable to the yield strength of ~ 3 GPa inferred for wadsleyite by Chen et al. (1998) at 600°C using in situ X-ray measurements of the relaxation of stress in powder samples compressed to 10 GPa. A coincidence in yield strengths at temperatures 500°C apart is not implausible if low-temperature plasticity is the dominant deformation mechanism, because the yield strength should be relatively temperature-insensitive in this regime. A comparison between our technique and that of Chen et al. (1998) is far from straightforward however, because the deformation mechanisms and imposed stress and strain rate conditions could be quite different for the two types of experiment.

For instance, recent microstructural examination of samples used for the in situ stress relaxation studies (Raterron et al., 1999) suggests that the samples experienced severe grain-size reduction, to the order of tens of nanometers, and acquired high defect densities as a result of cold-pressing (cf. Brearley et al., 1992). If this is the case, the apparent stress drop measured at 600°C by Chen et al. (1998) may be a manifestation of the relaxation of elastic strain energy accompanying recrystallization of the highly disordered starting material. This process is likely to be much different than that encountered in this study.

5.2. Effects of fluids

It is well known that olivine can incorporate small amounts of water into its structure as hydrogen defects at high pressure, and that the structures of wadsleyite and ringwoodite can contain significantly greater amounts, up to several weight percent (e.g., Kohlstedt et al., 1996). Because portions of subducting slabs may contain water dissolved in these phases, an important question is whether trace amounts of hydrogen result in hydrolytic weakening of the high-pressure phases of olivine. The limited evidence available so far for hydrolytic weakening in wadsleyite is contradictory. Chen et al. (1998) observed only slight stress differences in their experiments for anhydrous and very hydrous (3.8 wt.% H_2O) samples of wadsleyite. The addition of only 500 ppm H_2O in the experiments of Kubo et al. (1998a,b), however, resulted in a significant increase in the growth rate of wadsleyite compared to ''nominally dry'' experiments in which the water content of wadsleyite was estimated to be 200 ppm (see Fig. 7). Our modeling of Kubo et al.'s (1998a,b) experiments suggests that the strength difference between the ''dry'' and ''wet'' samples is about 1 GPa (Fig. 7), lending support to their hypothesis of water weakening. An open question concerns the effects of water partitioning between the phases, which may be a major factor in the case of olivine and wadsleyite (cf. Young et al., 1993). Partitioning of water into wadsleyite may promote hydrolytic weakening during the transformation, but may also result in depletion of hydrogen at the interface between the phases, slowing the growth rate. The interplay between these

processes is difficult to distinguish in the experiments of Kubo et al. (1998a,b), where water infiltrated the samples during the experiments, and therefore clearly needs to be addressed in future studies.

5.3. Limitations of the technique

Unfortunately, the present state of the art in deformation experiments at transition zone pressures does not allow for simultaneous measurement of stress and strain rate (e.g., Karato and Rubie, 1997). The method described here is therefore potentially an attractive alternative to traditional deformation experiments for determining the strength of phases that undergo high-pressure phase transitions. In this section, we discuss some of the limitations of the technique.

A principle limitation is that only a limited window in pressure–temperature space can be investigated using this technique. At low temperatures, elastic strain energy does not relax and growth is too slow on experimental time scales. Conversely, at high temperatures, stress relaxation as well as growth rates may be too fast for any effect to be observed. Low pressures also present a problem because the technique requires high nucleation rates in order to obtain constant, symmetric reaction rims. Nucleation rates are well known to be exponentially dependent on ΔG_{rxn}, which is largely pressure-dependent for solid–solid phase transformations. Furthermore, the interface-controlled growth rate (Eq. 1) is also exponentially dependent on ΔG_{rxn}. At low oversteps of equilibrium, therefore, the growth rate is very sensitive to the value of ΔG_{rxn}. At present, there is a large uncertainty in this parameter for the $(Mg,Fe)_2SiO_4$ system given the uncertainties in the available thermodynamic data (Akaogi et al., 1989) as well as the uncertainty of pressure calibrations (Rubie, 1999). This problem may be especially relevant in modeling the experiments of Kubo et al. (1998a,b), which were conducted at lower pressures than our experiments and hence, lower oversteps of equilibrium. The sensitivity of growth rate to ΔG_{rxn} is a larger limitation than uncertainties in the activation energy parameters, because the latter can effectively be made self-consistent for any given $P-T$ condition by modeling the early stages of growth (which are not affected by the accumulation of strain energy).

There may also be limitations in using the technique at higher pressures. For instance, previous studies have shown that the transformation of $(Mg,Fe)_2SiO_4$ olivine to its highest pressure polymorph, ringwoodite, proceeds by a complex mechanism involving intracrystalline nucleation and growth in addition to grain boundary nucleation and growth (Kerschhofer et al., 1996, 1998). Although the study of Liu et al. (1998) showed that rim growth is inhibited by elastic strain energy in these experiments, further study of this reaction at higher pressures is complicated by the possibility that the intracrystalline reaction products might impede the growth of the rim phase. Moreover, intracrystalline transformation could result in a pressure drop within the sample that would complicate the model. It therefore seems unlikely that this technique will work for determining the strength of $(Mg,Fe)_2SiO_4$ ringwoodite, although it may be possible to use the method for other compositions in which intracrystalline transformation does not predominate.

A more fundamental issue concerns the choice of mechanisms for relaxation of the rim phase. Our model is based on a simple mechanism of ideal plasticity. This approximation is reasonable in the case of low-temperature plasticity, in which the strain rate is highly sensitive to stress and is controlled by the rate of dislocation glide. Although we have not conclusively demonstrated that the wadsleyite rims deform by low-temperature plasticity, it is possible that deformation could be controlled by the rate of glide even though climb appears to be rapid. Such a model for low-temperature plasticity has been derived for metals (Weertman, 1957). Dislocation glide can occur in wadsleyite via glide of $\langle 101 \rangle$ partial dislocations on (010), thereby forming (010) stacking faults (Price, 1983; Sharp et al., 1994). However, the (010) stacking faults in our samples could also have formed as growth defects with [010] displacements. In principle, it may be possible to differentiate between these possibilities using HRTEM.

5.4. Implications for olivine metastability

Our results suggest that current models (Rubie and Ross, 1994; Däßler et al., 1996; Kirby et al., 1996) of olivine metastability, which are based on the assumption that growth rates of wadsleyite and

ringwoodite are constant at fixed *P* and *T*, may need to be revised to take into account the inhibition of growth by transformation strain energy. As noted previously by Liu et al. (1998), the effect of strain energy on growth rates is greatest when continuous reaction rims form around olivine grains, as in the experimental studies discussed above. Such a microstructure (see Fig. 9 in Liu et al., 1998) will develop when grain boundary nucleation kinetics are fast and growth kinetics are slow, as predicted by the model of Rubie and Ross (1994) for some cold subducting slabs. After an initial period of linear, interface-controlled growth, the growth kinetics may thus be controlled by the rate of stress relaxation. The overall effect would be to widen the depth interval over which transformation occurs, while the depth at which transformation begins should not be affected.

Unfortunately, neither our data nor the results of other studies (e.g., Chen et al., 1998) are precise enough to develop reliable flow-laws for wadsleyite and ringwoodite, needed to predict the effect of transformation stress at low temperatures (500 to 700°C) in subducting slabs. Nevertheless, to illustrate the potential importance of the phenomenon, we have modeled (Fig. 8) the growth rate of a reaction rim (in this case ringwoodite) on a 5-mm grain of olivine at 600°C and 15 GPa, a typical set of parameters used in the models of Rubie and Ross (1994). As shown in the figure, growth is inhibited significantly on geological time scales if the yield strength of ringwoodite is greater than about 2 GPa at these conditions. Note that realistic modification of the

thermokinetic models would be considerably more complicated, even if the flow-laws were well constrained, because transformation is of course non-isobaric and non-isothermal along any given *P–T* path for a slab subducting at a given velocity.

6. Conclusions

We have described and applied a new technique for determining the strength of high-pressure phases based on the interaction between kinetics and rheology during transformation. Moreover, we have demonstrated that transformation stress is a potentially important factor inhibiting growth kinetics during high-pressure transformations. Although limitations discussed above make it qualitative compared to high-resolution deformation experiments, this method can provide some constraints on rheology at conditions under which completely quantitative deformation tests (which measure simultaneous stress and strain rate) are currently impossible to perform because of technical limitations.

The results imply a significant increase in strength attending the transformation of olivine to wadsleyite, provided the deformation mechanism is identical to that of the experiments. Thermomechanical (Davies, 1995) and thermokinetic (Rubie and Ross, 1994; Däßler et al., 1996; Kirby et al., 1996) models of ''cold'' subducting slabs indicate that the temperatures, stresses, and strain rates at which the transformation takes place are such that low-temperature plasticity should dominate, consistent with an increase in strength based on our results. In the coldest regions of slabs, however, grain-size reduction accompanying the transformation may change the deformation mechanism to grain-size dependent diffusion creep, resulting in a reduction in strength (Rubie, 1984; Riedel and Karato, 1997). Such a strength reduction will be transient because grain growth of the high-pressure phase results in a return to the low-temperature plasticity regime.

The extent of olivine metastability in subducting slabs has been predicted using thermokinetic models (Rubie and Ross, 1994; Däßler et al., 1996; Kirby et al., 1996). These models are based on the assumption that growth rates of the high-pressure polymorphs, wadsleyite and ringwoodite, are constant at
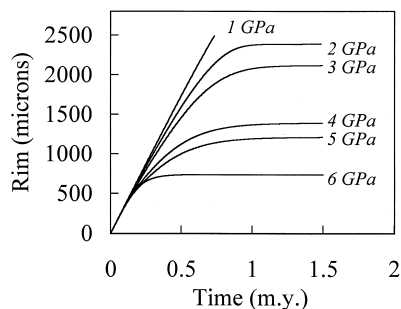

Fig. 8. Model fits at 600°C and 15 GPa assuming various yield strengths for ringwoodite, for an initial olivine grain size of 5 mm. Strain energy accumulation exerts a significant effect on growth for strengths greater than or equal to about 2 GPa.

fixed P and T. Our results clearly show that this assumption is invalid at 1100°C due to the accumulation of strain energy. Whether or not strain energy controls growth kinetics at lower temperatures (500–700°C) during subduction depends on the rheology, which currently cannot be estimated reliably by extrapolation. Moreover, although strain energy accumulation would broaden the depth interval over which the phase transformation occurs, it should have little or no effect on the depth at which transformation starts.

Acknowledgements

Appendix A. Elasto-plastic model for time-dependent growth rates

Here we solve for the stress and strain field in a system in which a wadsleyite rim grows into an initially spherical olivine grain. We employ spherical coordinates to exploit the symmetry of the problem. Because the deformation is irrotational, tangential displacements and off-diagonal components of the stress tensor are zero in this coordinate system. The equalities of the tangential components of the deviatoric stress ($\sigma_\phi = \sigma_\theta$) and strain ($e_\phi = e_\theta$) tensors are implicitly assumed hereafter. The components of the strain tensor can then be expressed in terms of the radial displacement u:

$$e_r = \frac{du}{dr}, \quad e_\theta = \frac{u}{r} \tag{A1}$$

In the elastic zone of the wadsleyite rim, mechanical equilibrium requires that the radial displacements satisfy the equation $u = C_1 r + C_2 / r^2$. Therefore, the components of the strain tensor can be expressed as:

$$e_r = C_1 - 2C_2 / r^3, \quad e_\theta = C_1 + C_2 / r^3 \tag{A2}$$

Using Hooke's law, Eq. A2 can be rewritten in terms of the radial and tangential deviatoric stresses within the elastic zone (i.e., $r_p < r < R$):

$$\sigma_r^e = 3KC_1 - \frac{4C_2\,\mu}{r^3}, \quad \sigma_\theta^e = 3KC_1 + \frac{2C_2\,\mu}{r^3} \tag{A3}$$

where K and μ are the bulk and shear moduli. The boundary conditions:

$$\sigma_r = 0 \text{ at } r = R \tag{A4}$$

$$\sigma_r = \sigma_\theta - \sigma_y \text{ for } a < r \le r_p, \tag{A5}$$

where σ_y is the yield strength, determine the constants C_1 and C_2 as:

$$C_1 = \frac{4}{3} \frac{\mu}{K} \frac{C_2}{R^3}, \quad C_2 = \frac{r_p^3}{6} \frac{\sigma_y}{\mu}. \tag{A6}$$

Within the elastoplastic zone, the differential stress $\sigma_\theta - \sigma_r$ is constrained by the yield strength (Eq. A7). Thus, the condition for stress equilibrium:

$$\frac{d\sigma_r}{dr} = \frac{2(\sigma_\theta - \sigma_r)}{r} \tag{A7}$$

can be written in terms of the yield strength and integrated to obtain the radial component of the deviatoric stress tensor in the elastoplastic zone:

$$\sigma_r^p = \sigma_{r,r=r_p} + 2\sigma_y \ln\left(\frac{r}{r_p}\right). \tag{A8}$$

Contiguity of the stress tensor at the boundary between the elastic and elastoplastic zones together with Eqs. A3 and A6 yields:

$$\sigma_{r,r=r_p} = \frac{2}{3}\sigma_y\left(\frac{r_p^3}{R^3} - 1\right) \tag{A9}$$

Strains in the plastic zone can be expressed as the sum of elastic and plastic components:

$$e_r = \frac{du}{dr} = e_r^e + e_r^p \tag{A10a}$$

$$e_\theta = \frac{u}{r} = e_\theta^e + e_\theta^p \tag{A10b}$$

By introducing the incompressibility condition for the plastic strains $e_r^p + 2e_\theta^p = 0$ and using Hooke's

law together with Eqs. A5 and A8 to express the elastic strain components in terms of stresses, Eqs. A10a and A10b can be combined to obtain:

$$\frac{du}{dr} + \frac{2u}{r} = \frac{2\sigma_y}{K}\left(\ln\left(\frac{r}{r_p}\right) + \frac{1}{3}\frac{r_p^3}{R^3}\right). \quad (A11)$$

The solution of Eq. A11 gives the displacement in the plastic zone as:

$$u_p = \frac{2r\sigma_y}{3K}\left(\ln\left(\frac{r}{r_p}\right) + \frac{1}{3}\frac{r_p^3}{R^3} - \frac{1}{3}\right) + \frac{C_3}{r^2} \quad (A12)$$

Continuity requires that at $r = r_p$ the radial displacement in the plastic zone must be equal to the radial displacement in the elastic zone given by Eq. A1, thus the constant C3 in Eq. A12 is:

$$C_3 = \frac{\gamma r_p^3}{2} \quad (A13)$$

with $\gamma = \sigma_y(2\mu + 3K)/(9K\mu)$. From (Eqs. A10a, A10b and A12), the strains in the elastoplastic zone are:

$$e_r = \frac{2\sigma_y}{3K}\left(\frac{1}{3}\frac{r_p^3}{R^3} + \frac{2}{3} + \ln\left(\frac{r}{r_p}\right)\right) - \gamma\frac{r_p^3}{r^3} \quad (A14a)$$

$$e_\theta = \frac{2\sigma_y}{3K}\left(\frac{1}{3}\frac{r_p^3}{R^3} - \frac{1}{3} + \ln\left(\frac{r}{r_p}\right)\right) - \frac{\gamma}{2}\frac{r_p^3}{r^3}. \quad (A14b)$$

If the elastic components of the total strain are expressed in terms of stress, the radial plastic component of the total strain obtained from Eqs. A10a and A14a is:

$$e_r^p = \gamma\left(1 - \frac{r_p^3}{r^3}\right). \quad (A15)$$

Under the constraint of the rim, the radius of the inclusion is $a(1 + \beta\varepsilon)$, where β is an unknown factor determined by the elastoplastic deformation required to establish mechanical equilibrium. Thus, if the initial condition is taken to be the state when the inclusion has been placed in the hole of radius a in the matrix, the radial displacements within the inclusion are:

$$u_i = \beta\varepsilon r \quad (A16)$$

However, the inclusion must be compressed to reduce its initial radius from $a(1 + \varepsilon)$ to a, therefore the displacements within the inclusion relative to its unstressed state are:

$$u'_i = (\beta - 1)\varepsilon r \quad (A17)$$

and the (hydrostatic) strains from Eqs. A1 and A17 are:

$$e_r = e_\theta = (\beta - 1)\varepsilon. \quad (A18)$$

Applying Hooke's law for Eq. A18, the hydrostatic stress in the inclusion is:

$$\sigma_r = \sigma_\theta = 3(\beta - 1)\varepsilon K_i \quad (A19)$$

where K_i is the bulk modulus of the inclusion. Mechanical equilibrium requires contiguity of the radial stress components given by Eqs. A12 and A16 at the interface between the inclusion and the plastic zone at $r = a$. Thus, β can be expressed in terms of r_p:

$$\beta = 1 + \frac{2\sigma_y}{9\varepsilon K_i}\left(\frac{r_p^3}{R^3} - 1 + 3\ln\left(\frac{a}{r_p}\right)\right). \quad (A20)$$

The unknown outer radius of the elastoplastic zone r_p is determined by the boundary condition that the displacements at the boundary of the inclusion given by Eqs. A13 and A18 at $r = a$ must be equal:

$$\varepsilon = \frac{2}{9}\sigma_y\left(\frac{1}{K_i} - \frac{1}{K}\right)\left(\frac{r_p^3}{R^3} - 1 + 3\ln\left(\frac{a}{r_p}\right)\right) + \frac{\gamma}{2}\frac{r_p^3}{r^3}. \quad (A21)$$

Eq. A21 is transcendental and must be solved numerically. Once r_p is known, C_1 and C_2 (Eq. A6), β (Eq. A20) and $\sigma_{r,r=r_p}$ (Eq. A9) can be found analytically and used to obtain the components of the strain and deviatoric stress tensor within the olivine inclusion (Eqs. A18 and A19), and the elastoplastic (Eqs. A8, A14a, and A14b) and elastic (Eqs. A2 and A3) zones of the wadsleyite rim.

If the misfit strain ε is small such that the differential stress at the olivine–wadsleyite interface does not exceed the yield strength, then the entire shell deforms elastically. In this case, the differential stress at the interface is:

$$\sigma_e = \sigma_\theta - \sigma_r = \frac{18\varepsilon K_i}{4\frac{a^3}{R^3}\frac{K_i - K}{K} + 4 + 3\frac{K_i}{K}} \quad (A22)$$

and the components of the strain and stress tensor within the entire wadsleyite shell are given by Eqs. A2 and A3 with:

$$C_1 = \frac{4}{3} \frac{\mu}{K} \frac{C_2}{R^3}, \qquad C_2 = \frac{\sigma_e a^3}{6\mu}. \tag{A23}$$

Likewise, within the olivine Eqs. A18 and A19 apply with:

$$\beta = 1 + \frac{4 C_2 \mu}{3 \varepsilon K_i} \left(\frac{1}{R^3} - \frac{1}{a^3} \right). \tag{A24}$$

If the misfit strain is large, then the entire shell yields plastically. In this case, the equations for the general case apply with $r_p = R$ and $\sigma_{r,r=r_p} = 0$.

Finally, the strain energy of the olivine–wadsleyite assembly can be expressed as the sum of four components, the strain energy of the olivine inclusion:

$$W_i = \frac{4\pi a^3}{3} \left(\frac{3}{2} \sigma_r e_r \right) = 6\pi a^3 \varepsilon^2 K_i (\beta - 1)^2, \tag{A25}$$

the plastic strain energy of the elastoplastic zone:

$$W_p = -4\pi \int_a^{r_p} \sigma_y e_r^p r^2 \mathrm{d}r$$
$$= \frac{4\pi}{3} \gamma \sigma_y \left(a^3 - r_p^3 - 3 r_p^3 \ln\left(\frac{a}{r_p} \right) \right), \tag{A26}$$

the elastic strain energy of the elastoplastic zone:

$$W_e = 4\pi \int_a^r \left(\frac{1}{2} \left(\sigma_r (e_r - e_r^p) + 2\sigma_\theta (e_\theta - e_\theta^p) \right) \right) r^2 \mathrm{d}r$$
$$= -\frac{W_p}{2} + 4\pi \int_a^r \left(\frac{1}{2} \left(\sigma_r (e_r + e_\theta) + 2\sigma_y e_\theta \right) \right) r^2 \mathrm{d}r$$
$$= -\frac{W_p}{2} + \frac{4\pi \sigma_y}{3K} \left(\frac{2}{9} \sigma_y \left(\frac{r_p^6}{R^6} - 2 \frac{r_p^3}{R^3} + 1 \right) \right.$$
$$\times \left(r_p^3 - a^3 \right) + \ln\left(\frac{a}{r_p} \right) \left(2 a^3 \sigma_y \left(\frac{2}{3} - \frac{2}{3} \frac{r_p^3}{R^3} \right. \right.$$
$$\left. \left. \left. - \ln\left(\frac{a}{r_p} \right) \right) - \frac{3}{2} \gamma r_p^3 K \right) \right) \tag{A27}$$

and the elastic strain energy of the outer elastic zone:

$$W_o = 4\pi \int_a^{r_p} \frac{1}{2} \left(\sigma_r e_r + 2\sigma_\theta e_\theta \right) r^2 \mathrm{d}r$$
$$= 2\pi \left(3 C_1^2 K \left(R^3 - r_p^3 \right) - 4 C_2^2 \mu \left(\frac{1}{R^3} - \frac{1}{r_p^3} \right) \right) \tag{A28}$$

where C_1 and C_2 are given by Eq. A6 if the elastoplastic zone exists, and by Eq. A23 with $r_p = a$ otherwise.

References

Agee, C.A., Walker, D., 1988. Mass balance and phase density constraints on early differentiation of chondritic mantle. Earth Planet. Sci. Lett. 90, 144–156.

Akaogi, M., Ito, E., Navrotsky, A., 1989. Olivine-modified spinel–spinel transitions in the system Mg_2SiO_4–Fe_2SiO_4: calorimetric measurements, thermochemical calculation, and geophysical application. J. Geophys. Res. 94, 15671–15685.

Ando, J., Irifune, T., Takeshita, T., Fujino, K., 1997. Evaluation of the non-hydrostatic stress produced in a multi-anvil high pressure apparatus. Phys. Chem. Miner. 24, 139–148.

Ashby, M.F., Verrall, R.A., 1973. Diffusion accommodated flow and superplasticity. Acta Metall. 21, 149–163.

Brearley, A.J., Rubie, D.C., Ito, E., 1992. Mechanisms of the transformations between the alpha, beta and gamma polymorphs of Mg2SiO4 at 15 GPa. Phys. Chem. Miner. 18, 343–358.

Carlson, W.D., Rosenfeld, J.L., 1981. Optical determination of topotactic aragonite–calcite growth kinetics: metamorphic implications. J. Geol. 89, 615–638.

Chen, J., Inoue, T., Weidner, D.J., Wu, Y., Vaughan, M., 1998. Strength and water weakening of mantle minerals, olivine, wadsleyite, and ringwoodite. Geophys. Res. Lett. 25, 575–578.

Christian, J.W., 1975. The Theory of Transformations in Metals and Alloys. Pergamon, Oxford, 586 pp.

Däßler, R., Yuen, D.A., Karato, S., Riedel, M.R., 1996. Two-dimensional thermo-kinetic model for the olivine–spinel phase transition in subducting slabs. Phys. Earth Planet. Inter. 94, 217–239.

Davies, G.F., 1995. Penetration of plates and plumes through the mantle transition zone. Earth Planet. Sci. Lett. 133, 507–516.

Dupas-Bruzek, C., Sharp, T.G., Rubie, D.C., Durham, W.B., 1998a. Mechanisms of transformation and deformation in $Mg_{1.8}Fe_{0.2}SiO_4$ olivine and wadsleyite under non-hydrostatic stress. Phys. Earth Planet. Inter. 108, 33–48.

Dupas-Bruzek, C., Tingle, T.N., Green, H.W. II, Doukhan, N., Doukhan, J.-C., 1998b. The rheology of olivine and spinel magnesium germanate (Mg_2GeO_4): TEM study of the defect microstructures. Phys. Chem. Miner. 25, 501–514.

Frost, H.J., Ashby, M.F., 1982. Deformation-mechanism Maps. Pergamon, Tarrytown, NY.

Gillet, P., Gerard, Y., Willaime, C., 1987. The calcite–aragonite

transition: mechanism and microstructures induced by the transformation stress and strain. Bull. Mineral. 110, 481–496.

Green, H.W., Young, T.E., Walker, D., Scholz, C.H., 1992. The effect of nonhydrostatic stress on the $\alpha \rightarrow \beta$ and $\alpha \rightarrow \gamma$ olivine phase transformations. In: Syono, Y., Manghnani, M.H. (Eds.), High Pressure Research: Application to Earth and Planetary Sciences. American Geophysical Union, Washington, pp. 229–235.

Hill, R., 1950. The Mathematical Theory of Plasticity. Oxford Univ. Press, Oxford, 356 pp.

Honda, K., Sato, M., 1954. On the theory of transformation stress. In: Reactivity of Solids. Proc. 2nd Int. Symp. on the Reactivity of Solids, Gothenburg. pp. 847–857.

Karato, S., 1997. Phase transformations and rheological properties of mantle minerals. In: Crossley, D.J. (Ed.), Earth's Deep Interior 7 Gordon & Breach, Amsterdam, 7, pp. 223–272.

Karato, S., Dupas-Bruzek, C., Rubie, D.C., 1998. Plastic deformation of silicate spinel under the transition-zone conditions of the Earth's mantle. Nature 395, 266–269.

Karato, S., Rubie, D.C., 1997. Toward an experimental study of deep mantle rheology: a new multianvil sample assembly for deformation studies under high pressures and temperatures. J. Geophys. Res. 102, 20111–20122.

Katsura, T., Ito, E., 1989. The system $Mg_2SiO_4 – Fe_2SiO_4$ at high pressures and temperatures: precise determination of the stabilities of olivine, modified spinel and spinel. J. Geophys. Res. 94, 15663–15670.

Kerschhofer, L., Dupas, C., Liu, M., Sharp, T.G., Durham, W.B., Rubie, D.C., 1998. Polymorphic transformations between olivine, wadsleyite and ringwoodite: mechanisms of intracrystalline nucleation and the role of elastic strain. Mineral. Mag. 62, 617–638.

Kerschhofer, L., Sharp, T.G., Rubie, D.C., 1996. Intracrystalline transformation of olivine to wadsleyite and ringwoodite under subduction zone conditions. Science 274, 79–81.

Kirby, S.H., Stein, S., Okal, E.A., Rubie, D.C., 1996. Metastable mantle phase transformations and deep earthquakes in subducting lithosphere. Rev. Geophys. 34, 261–306.

Kohlstedt, D.L., Keppler, H., Rubie, D.C., 1996. Solubility of water in the α, β, and γ phases of $(Mg, Fe)_2SiO_4$. Contrib. Mineral. Petrol. 123, 345–357.

Kubo, 1998. Transformation kinetics of mantle minerals. PhD Thesis, Tohoku University, 167 pp.

Kubo, T., Ohtani, E., Kato, T., Shinmei, T., Fujino, K., 1998a. Experimental investigation of the $\alpha – \beta$ transformation of San Carlos olivine single crystal. Phys. Chem. Miner. 26, 1–6.

Kubo, T., Ohtani, E., Shinmei, T., Fujino, K., 1998b. Effects of water on the $\alpha – \beta$ transformation kinetics in San Carlos olivine. Science 281, 85–87.

Lee, J.K., Earmme, Y.Y., Aaronson, H.I., Russell, K.C., 1980. Plastic relaxation of the transformation strain energy of a misfitting spherical precipitate: ideal plastic behavior. Metall. Trans. A 11A, 1837–1847.

Liu, M., Kerschhofer, L., Mosenfelder, J., Rubie, D.C., 1998. The effect of strain energy on growth rates during the olivine–spinel transformation and implications for olivine metastability in subducting slabs. J. Geophys. Res. 103, 23897–23909.

Liu, M., Yund, R.A., 1995. The elastic strain energy associated with the olivine–spinel transformation and its implications. Phys. Earth Planet. Inter. 89, 177–197.

Martinez, I., Wang, Y., Guyot, F., Liebermann, R.C., 1997. Microstructures and iron partitioning in $(Mg,Fe)SiO_3$ perovskite and $(Mg,Fe)O$ assemblages: an analytical transmission electron microscope study. J. Geophys. Res. 102, 5265–5280.

Morishima, H., Kato, T., Suto, M., Ohtani, E., Urukawa, S., Utsumi, W., Shomomura, O., 1994. The phase boundary between α- and β-Mg_2SiO_4 determined by in situ X-ray diffraction. Science 265, 1202–1203.

Morris, S., 1992. Stress relief during solid-state transformations in minerals. Proc. R. Soc. London, Ser. A 436, 203–216.

Morris, S., 1995. The relaxation of a decompressed inclusion. Z. Angew. Math. Phys. 46, S335–S355.

Mosenfelder, J.L., Bohlen, S.R., 1997. Kinetics of the coesite to quartz transformation. Earth Planet. Sci. Lett. 153, 133–147.

Price, G.D., 1983. The nature and significance of stacking faults in wadsleyite, natural β-$(Mg,Fe)_2SiO_4$ from the Peace River meteorite. Phys. Earth Planet. Inter. 33, 137–147.

Raterron, P., Wu, Y., Weidner, D.J., 1999. Olivine plastic instability as an alternative process for deep focus earthquakes? TEM investigation of high pressure olivine samples exhibiting stress instabilities above 400°C. EOS, Trans. Am. Geophys. Union 80, 974.

Remsberg, A.R., Boland, J.N., Gasparik, T., Liebermann, R.C., 1988. Mechanism of the olivine–spinel transformation in Co_2SiO_4. Phys. Chem. Miner. 15, 498–506.

Riedel, M.R., Karato, S., 1997. Grain-size evolution in subducted oceanic lithosphere associated with the olivine–spinel transformation and its effects on rheology. Earth Planet. Sci. Lett. 148, 27–43.

Rubie, D.C., 1984. The olivine–spinel transformation and the rheology of subducting lithosphere. Nature 308, 505–508.

Rubie, D.C., 1999. Characterising the sample environment in multianvil high-pressure experiments. Phase Trans. 68, 431–451.

Rubie, D.C., Champness, P.E., 1987. The evolution of microstructure during the transformation of Mg_2GeO_4 olivine to spinel. Bull. Mineral. 110, 471–480.

Rubie, D.C., Karato, S., Yan, H., O'Neill, H.S.C., 1993. Low differential stress and controlled chemical environment in multianvil high-pressure experiments. Phys. Chem. Miner. 20, 315–322.

Rubie, D.C., Ross, C.R. II, 1994. Kinetics of the olivine–spinel transformation in subducting lithosphere: experimental constraints and implications for deep slab processes. Phys. Earth Planet. Inter. 86, 223–241.

Rubie, D.C., Thompson, A.B., 1985. Kinetics of metamorphic reactions at elevated temperatures and pressures: an appraisal of experimental data. In: Thompson, A.B., Rubie, D.C. (Eds.), Metamorphic Reactions: Kinetics, Textures, and Deformation. Springer, New York.

Sharp, T.G., Bussod, G.Y.A., Katsura, T., 1994. Microstructures in β-$Mg_{1.8}Fe_{0.2}SiO_4$ experimentally deformed at transition-zone conditions. Phys. Earth Planet. Inter. 86, 69–83.

Turnbull, D., 1956. Phase changes. Solid State Phys. 3, 225–306.

Vaughan, P.J., Coe, R.S., 1981. Creep mechanism in Mg_2GeO_4: effects of a phase transition. J. Geophys. Res. 86, 389–404.

Weertman, J., 1957. Steady-state creep of crystals. J. Appl. Phys. 28, 1185–1189.

Weidner, D.J., Vaughan, M.T., Ko, J., Wang, Y., Liu, X., Yeganeh-Haeri, A., Pacalo, R.E., Zhao, Y., 1992. Characterization of stress, pressure, and temperature in SAM85, a DIA type high pressure apparatus. In: Syono, Y., Manghnani, M.H. (Eds.), High-Pressure Research: Application to Earth and Planetary Sciences. American Geophysical Union, Washington, pp. 13–17.

Weidner, D.J., Wang, Y., Vaughan, M.T., 1994. Yield strength at high pressure and temperature. Geophys. Res. Lett. 21, 753–756.

Young, T.E., Green, H.W. II, Hofmeister, A.M., Walker, D., 1993. Infrared spectroscopic investigation of hydroxyl in β-$(Mg,Fe)_2SiO_4$ and coexisting olivine: implications for mantle evolution and dynamics. Phys. Chem. Miner. 19, 409–422.

Zhang, J., Li, B., Utsumi, W., Liebermann, R.C., 1996. In situ X-ray observations of the coesite–stishovite transition: reversed phase boundary and kinetics. Phys. Chem. Miner. 23, 1–10.